Field-Induced Single-Molecule Magnets of Dysprosium Involving Quinone Derivatives

Konstantin Martyanov[1], Jessica Flores Gonzalez[2], Bertrand Lefeuvre[2], Vincent Dorcet[2], Vladimir Cherkasov[1], Olivier Cador[2], Viacheslav Kuropatov[1], Fabrice Pointillart[2]**

[1] G. A. Razuvaev Institute of Organometallic Chemistry of Russian Academy of Sciences, 603950, GSP-445, Tropinina str., 49, Nizhny Novgorod, Russia

[2] Univ Rennes, CNRS, ISCR (Institut des Sciences Chimiques de Rennes) - UMR 6226, F-35000 Rennes, France

* Correspondence: fabrice.pointillart@univ-rennes1.fr,

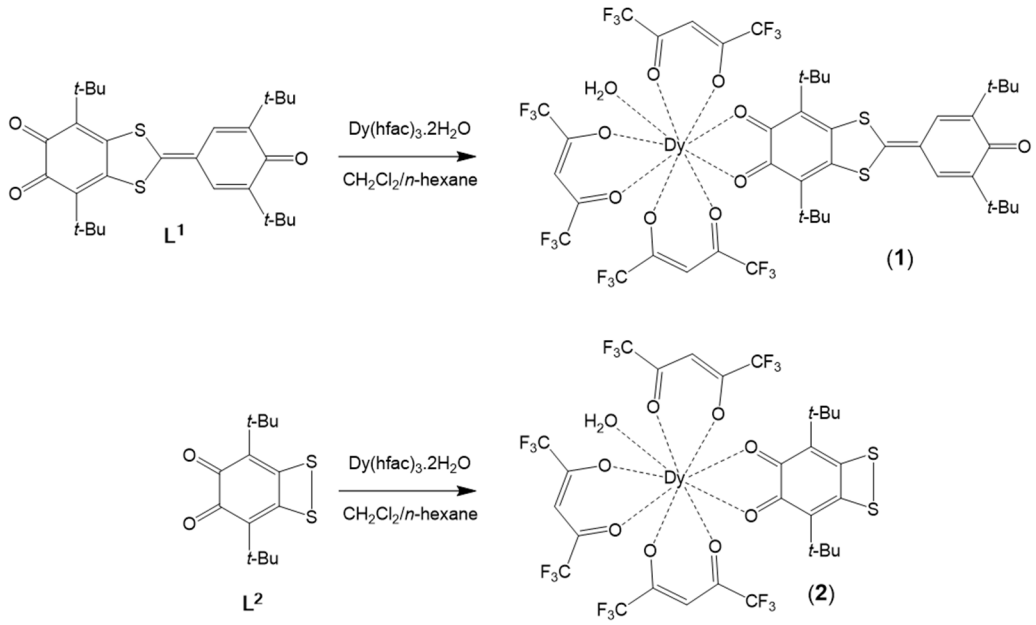

Scheme S1. Coordination reactions leading to the formation of complexes **1** and **2**.

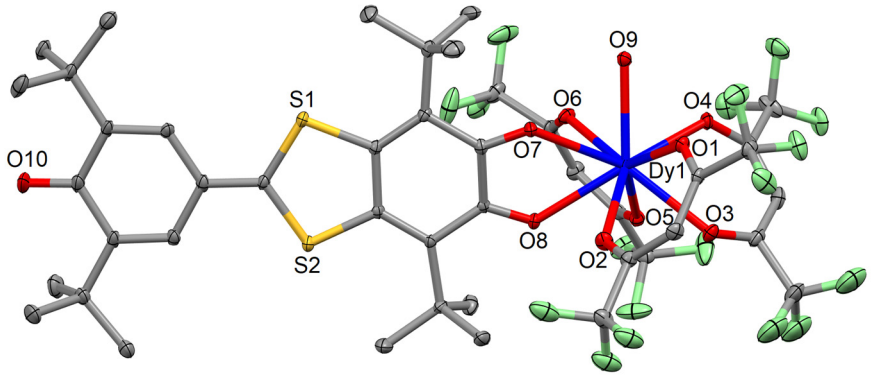

Figure S1. ORTEP view of the asymmetric unit for **1**. Thermal ellipsoids are drawn at 30% probability. Hydrogen atoms are omitted for clarity.

Table S1. X-ray crystallographic data of $\mathbf{L^1}$, **1** and **2**.

Compounds	$\mathbf{L^1}$	**1**	**2**·(C_6H_{14})(CH_2Cl_2)
Formula	$C_{29}H_{38}O_3S_2$	$C_{44}H_{43}DyF_{18}O_{10}S_2$	$C_{29}H_{23}DyF_{18}O_9S_2$
M / g.mol^{-1}	498.71	1300.39	1084.08
Crystal system	Tetragonal	Monoclinic	Monoclinic
Space group	P-4 (N°81)	C2/c (N°15)	$P2_1$ (N°4)
Cell parameters	a = 20.626(4) Å b = 20.626 Å c = 5.9732(15) Å	a = 36.383(3) Å b = 11.5164(9) Å c = 25.372(2) Å β = 104.059(3) °	a = 14.888(3) Å b = 24.124(4) Å c = 48.755(8) Å β = 94.137(6) °
Volume / Å^3	2541.2(11)	10312.3(15)	17466.0(50)
Z	4	8	16
T / K	150 (2)	150 (2)	150 (2)
2θ range /°	5.93 ≤ 2θ ≤ 54.96	5.98 ≤ 2θ ≤ 54.97	5.85 ≤ 2θ ≤ 54.97
ρ_{calc} / g.cm^{-3}	1.304	1.673	1.646
μ / mm^{-1}	0.239	1.648	1.927
Number of reflections	10474	11766	95325
Independent reflections	5463	11766	70496
$Fo^2 > 2\sigma(Fo)^2$	1878	10119	41234
Number of variables	164	684	1974
R_{int}, R_1, ωR_2	0.4417, 0.2473, 0.4546	0.0565, 0.0526, 0.1151	0.0741, 0.1244, 0.3060

Table S2. SHAPE analysis of the coordination polyhedron around the Dy(III) center for **1**.

	CShM$_{CSAPR-9}$ (C_{4v}, Spherical capped square antiprism)	CShM$_{TCTPR-9}$ (D_{3h}, Spherical tricapped trigonal prism)	CShM$_{MFF-9}$ (C_s, Muffin)
Dy1	0.385	1.258	0.871

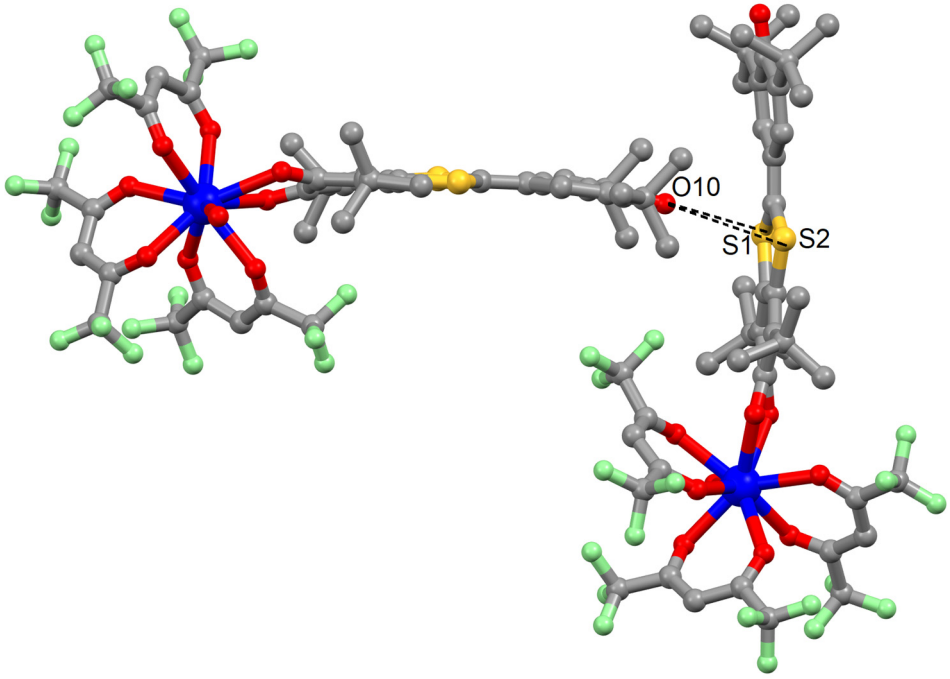

Figure S2. Orthogonal arrangement of two neighboring molecules in the crystal packing of **1**.

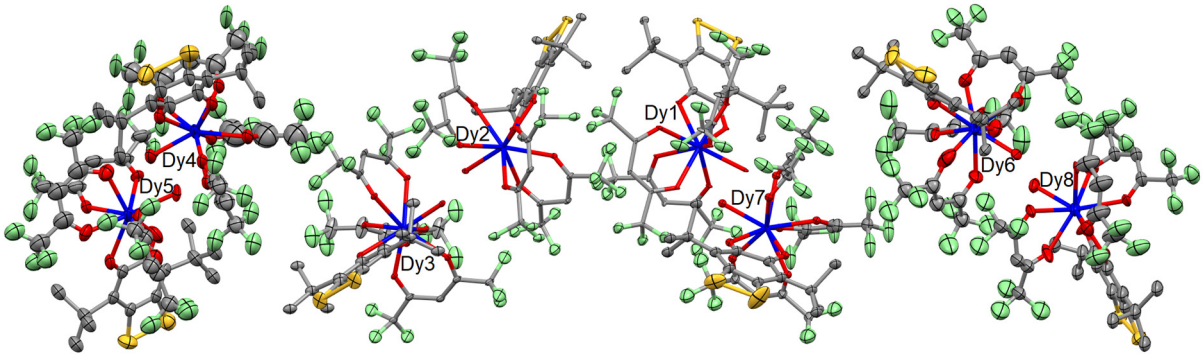

Figure S3. ORTEP view of the asymmetric unit for **2**·(C_6H_{14})(CH_2Cl_2). Thermal ellipsoids are drawn at 30% probability. Hydrogen atoms and solvent molecules of crystallization are omitted for clarity.

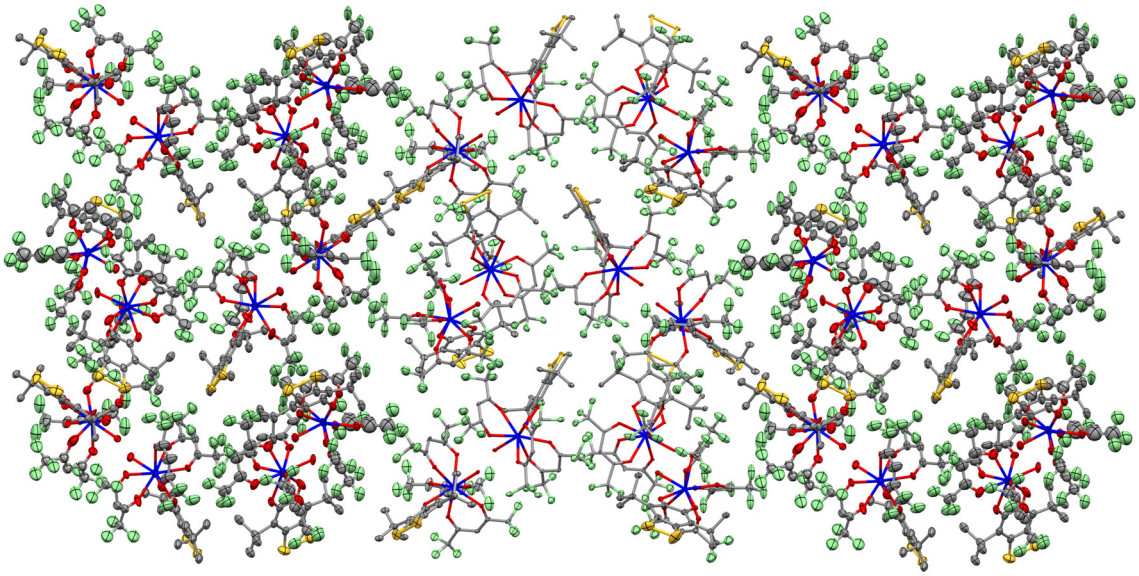

Figure S4. Crystal packing of **2**·(C_6H_{14})(CH_2Cl_2) showing the alternation between ordered and disordered layers of dimers.

Table S3. SHAPE analysis of the coordination polyhedra around the Dy(III) centers for **2**.

	$CShM_{TCTPR-9}$ (D_{3h}, Spherical tricapped trigonal prism)	$CShM_{CSAPR-9}$ (C_{4v}, Spherical capped square antiprism)	$CShM_{MFF-9}$ (C_s, Muffin)
Dy1	0.594	0.814	1.299
Dy2	0.536	0.907	1.330
Dy3	0.899	0.752	0.835
Dy4	1.296	0.737	0.920
Dy5	0.644	0.872	1.394
Dy6	0.977	0.704	0.917
Dy7	1.057	0.605	0.723
Dy8	0.720	0.673	1.153

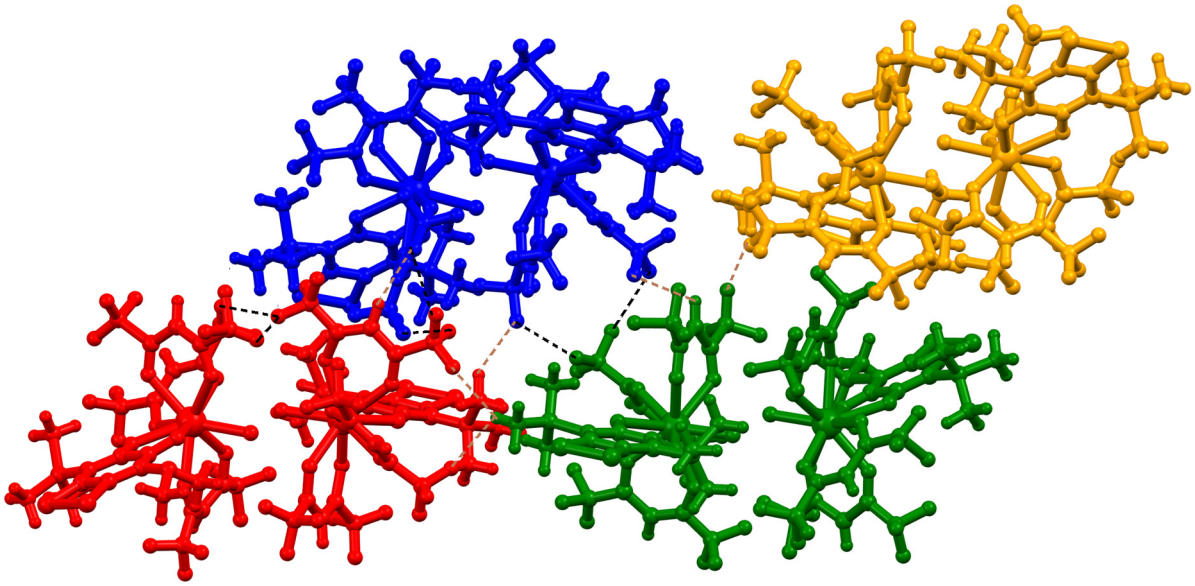

Figure S5. Representation of the four dimers constituting the asymmetric unit with H···F (dashed brown lines) and F···F (dashed black lines) contacts.

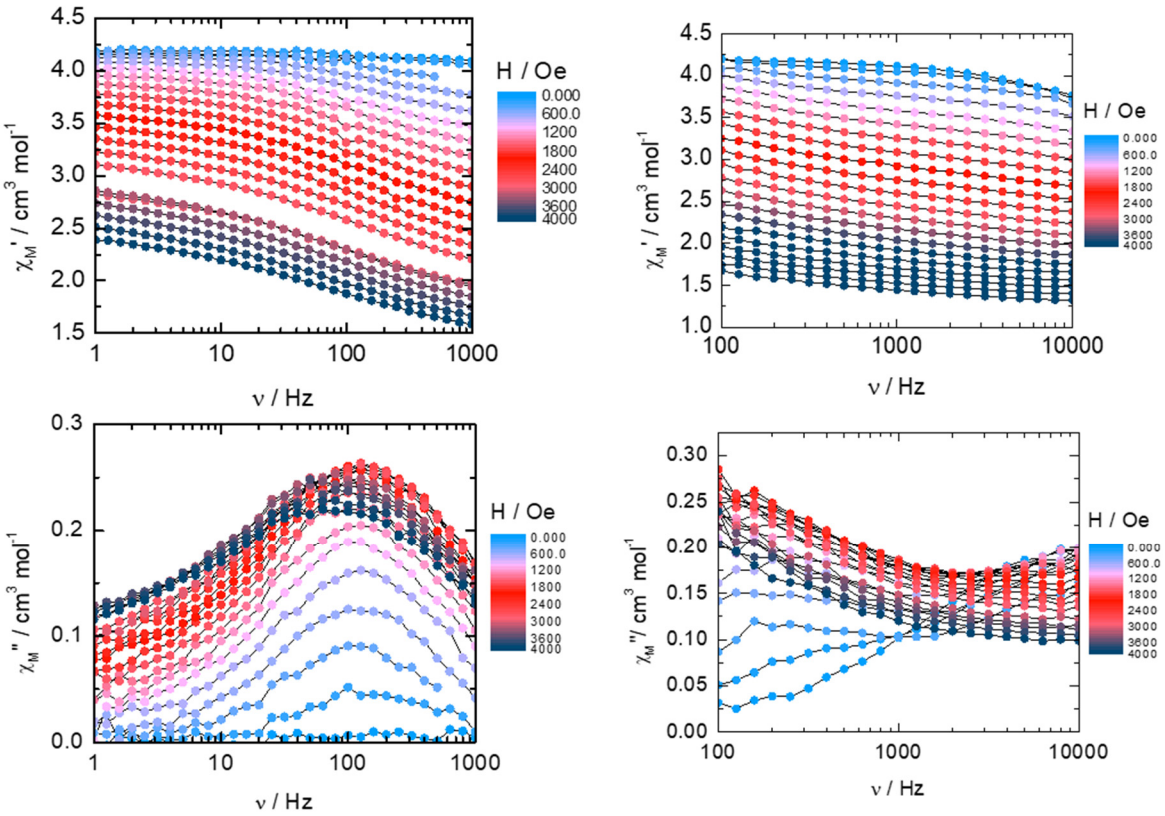

Figure S6. Field dependence of χ_M' and χ_M'' between 0 and 4000 Oe for **1** at 2K in the frequency range of 1-1000 Hz (left) and 100-10000 Hz (right).

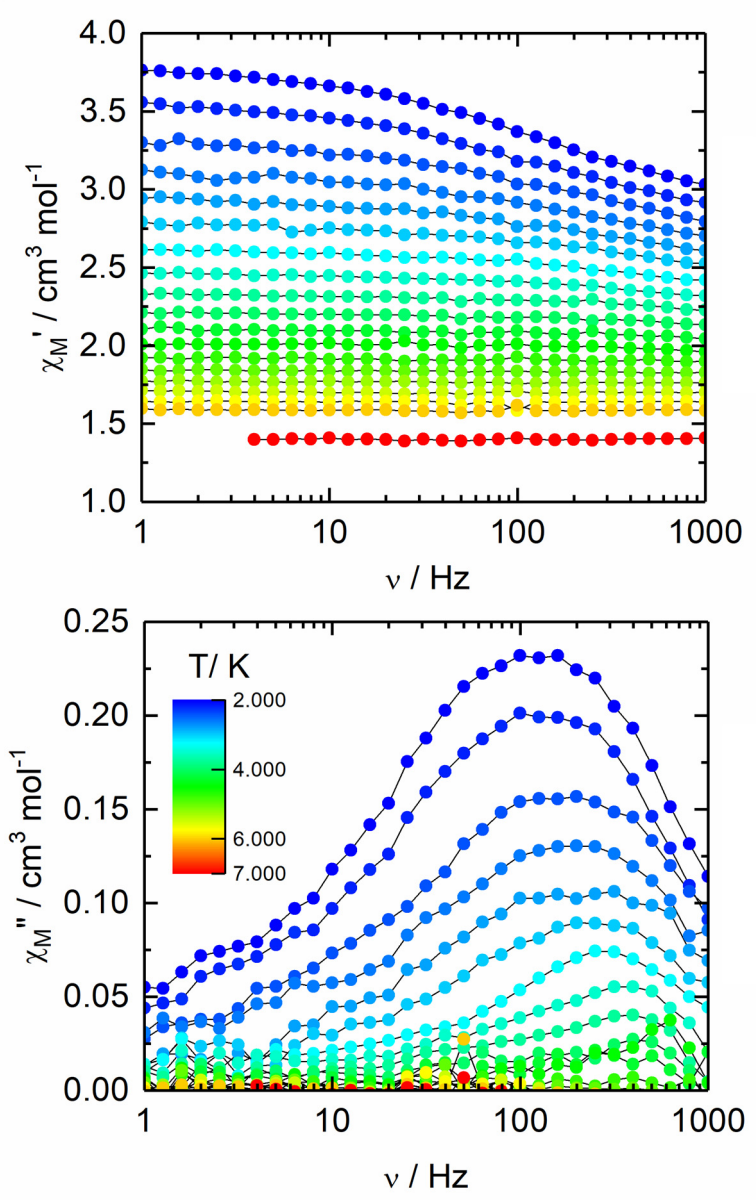

Figure S7. Frequency dependence of χ_M' (above) and χ_M'' (below) between 2 and 7 K at 1600 Oe for **1**.

Extended Debye model.

$$\chi_M' = \chi_S + (\chi_T - \chi_S)\frac{1+(\omega\tau)^{1-\alpha}\sin\left(\alpha\frac{\pi}{2}\right)}{1+2(\omega\tau)^{1-\alpha}\sin\left(\alpha\frac{\pi}{2}\right)+(\omega\tau)^{2-2\alpha}}$$

$$\chi_M'' = (\chi_T - \chi_S)\frac{(\omega\tau)^{1-\alpha}\cos\left(\alpha\frac{\pi}{2}\right)}{1+2(\omega\tau)^{1-\alpha}\sin\left(\alpha\frac{\pi}{2}\right)+(\omega\tau)^{2-2\alpha}}$$

With χ_T the isothermal susceptibility, χ_S the adiabatic susceptibility, τ the relaxation time and α an empiric parameter which describe the distribution of the relaxation time. For SMM with only one relaxing object α is close to zero. The extended Debye model was applied to fit simultaneously the experimental variations of χ_M' and χ_M'' with the frequency ν of the oscillating field ($\omega = 2\pi\nu$). Typically, only the temperatures for which a maximum on the χ'' vs. f curves, have been considered. The best fitted parameters τ, α, χ_T, χ_S are listed in Table S4 with the coefficient of determination R^2.

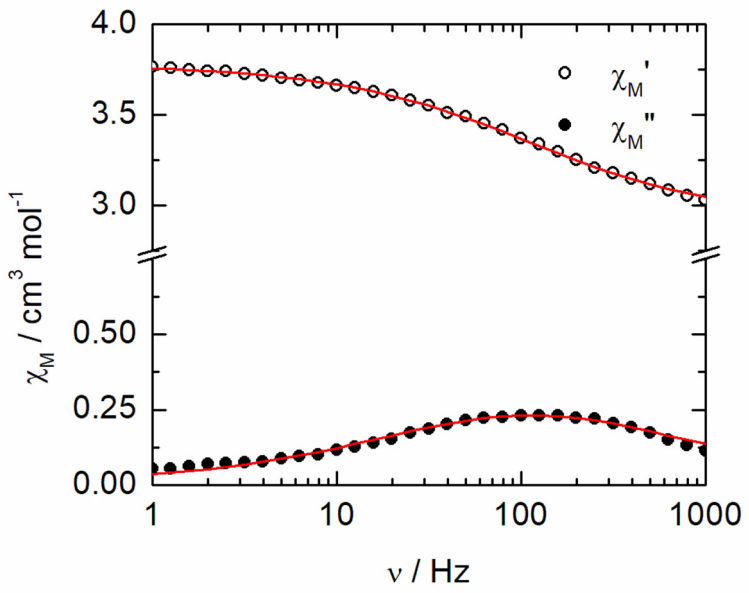

Figure S8. Frequency dependence of the in-phase (χ_M') and out-of-phase (χ_M'') components of the ac susceptibility measured on powder at 2 K and 1600 Oe with the best fitted curves (red lines) for **1**.

Table S4. Best fitted parameters (χ_T, χ_S, τ and α) with the extended Debye model for **1** at 1600 Oe in the temperature range 2-3.5 K.

T / K	χ_T / cm^3 mol^{-1}	χ_S / cm^3 mol^{-1}	α	τ / s	R^2
2	3.78223	2.91144	0.37668	0.00141	0.99997
2.2	3.54118	2.81513	0.36398	0.00133	0.99998
2.4	3.28211	2.71127	0.35448	9.65E-04	0.99997
2.6	3.10457	2.61645	0.37869	9.21E-04	0.99996
2.8	2.92807	2.53845	0.3567	8.03E-04	0.99997
3	2.7572	2.468	0.31079	6.57E-04	0.99997
3.25	2.57278	2.39629	0.12217	5.82E-04	0.99999
3.5	2.41533	2.31602	0.06909	4.87E-04	0.99999

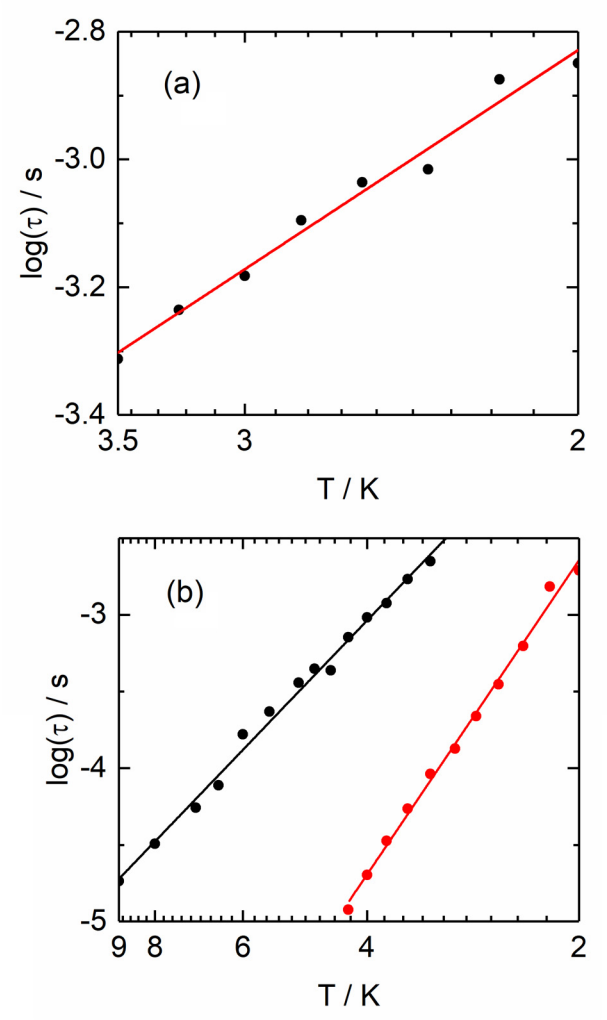

Figure S9. Linear plot of the ttemperature variation of the relaxation time for **1** (a) in the temperature range of 2-3.5 K and **2** (b) in the temperature range of 2-9 K with the best fitted curve with the modified Arrhenius law.

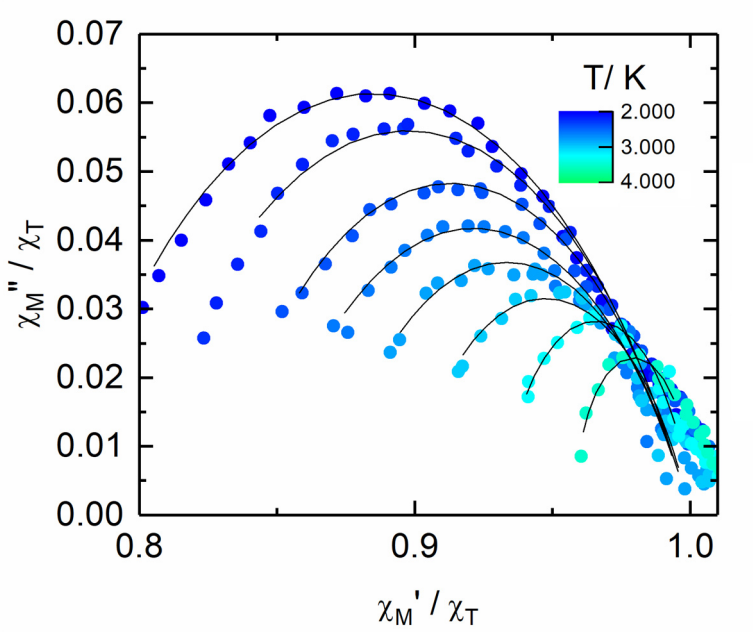

Figure S10. Normalized Argand plot for **1** between 2 and 4 K.

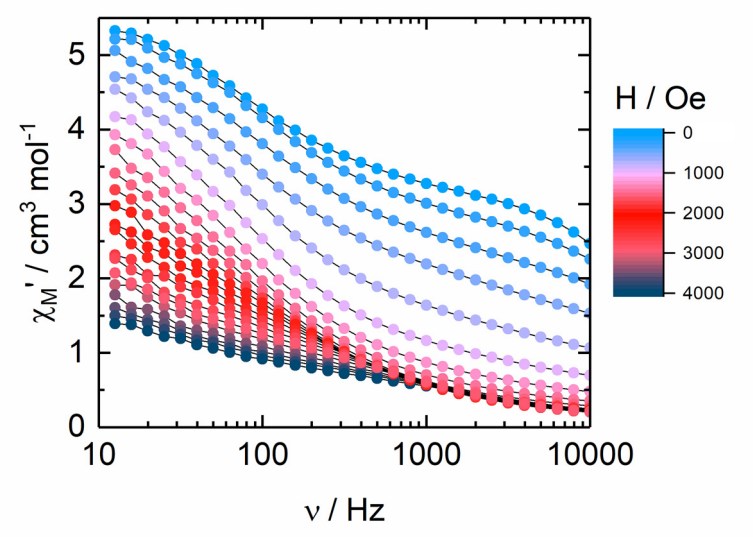

Figure S11. Frequency dependence of χ_M' between 0 and 4000 Oe for **2** at 2 K in the frequency range of 10-10000 Hz.

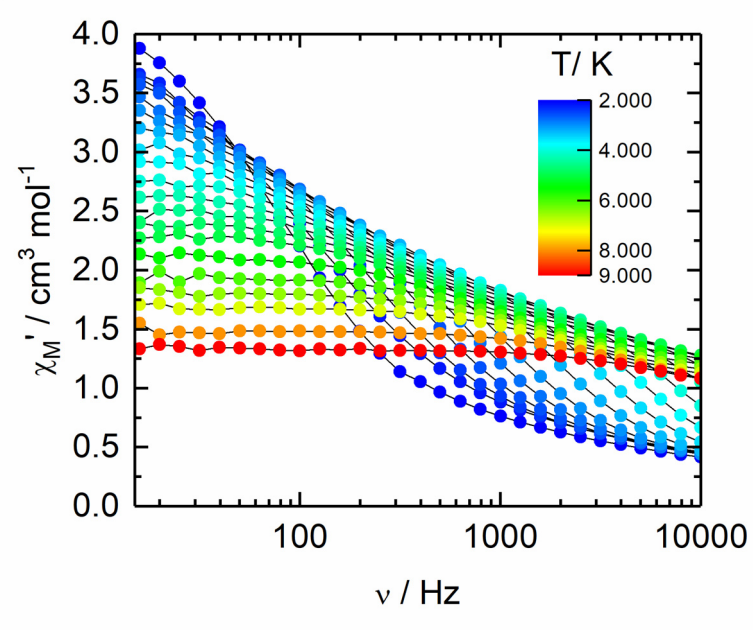

Figure S12. Frequency dependence of χ_M' between 2 and 9 K at 1200 Oe for **2**.

Extended Debye model.

$$\chi_M' = \chi_S + (\chi_T - \chi_S)\frac{1+(\omega\tau)^{1-\alpha}\sin\left(\alpha\frac{\pi}{2}\right)}{1+2(\omega\tau)^{1-\alpha}\sin\left(\alpha\frac{\pi}{2}\right)+(\omega\tau)^{2-2\alpha}}$$

$$\chi_M'' = (\chi_T - \chi_S)\frac{(\omega\tau)^{1-\alpha}\cos\left(\alpha\frac{\pi}{2}\right)}{1+2(\omega\tau)^{1-\alpha}\sin\left(\alpha\frac{\pi}{2}\right)+(\omega\tau)^{2-2\alpha}}$$

With χ_T the isothermal susceptibility, χ_S the adiabatic susceptibility, τ the relaxation time and α an empiric parameter which describe the distribution of the relaxation time. For SMM with only one relaxing object α is close to zero. The extended Debye model was applied to fit simultaneously the experimental variations of χ_M' and χ_M'' with the frequency ν of the oscillating field ($\omega = 2\pi\nu$). Typically, only the temperatures for which a maximum on the χ'' vs. f curves, have been considered. The best fitted parameters τ_1, α_1, χ_{1T}, τ_2, α_2, χ_{2T} and χ_S are listed in Table S5 with the coefficient of determination R^2. τ_1, α_1, χ_{1T}, χ_S are parameters for the low frequency contribution while τ_2, α_2, χ_{2T} and χ_S are for the high frequency contribution.

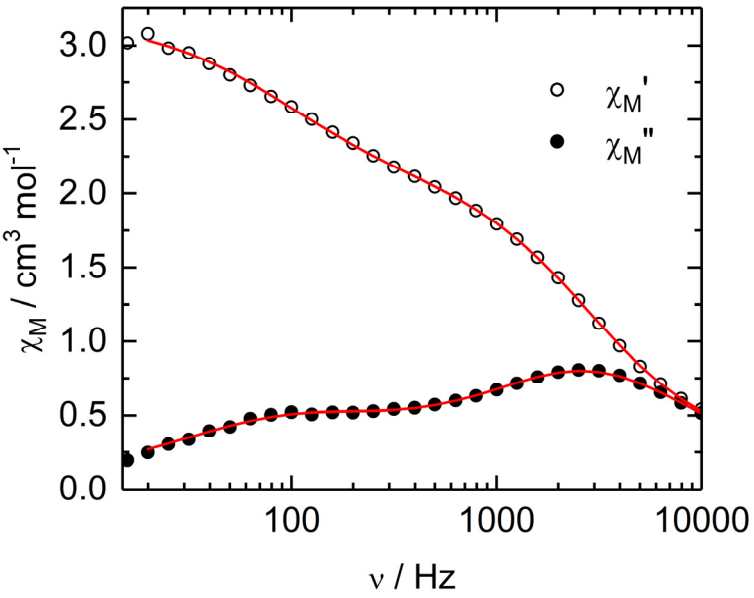

Figure S13. Frequency dependence of the in-phase (χ_M') and out-of-phase (χ_M") components of the ac susceptibility measured on powder at 3.5 K and 1200 Oe with the best fitted curves (red lines) for **2**.

Table S5. Best fitted parameters (τ_1, α_1, χ_{1T}, τ_2, α_2, χ_{2T} and χ_S) with the extended Debye model for **2** at 1200 Oe in the temperature range 2-9 K.

T/ K	χ_{1T}	τ_1	α_1	χ_{2T}	α_2	τ_2	χ_S
2				4.81622	0.27749	0.00195	0.81669
2.2				4.71919	0.33501	0.00153	0.75195
2.4				1.06979	0.01354	0.00062752	0.24618
2.6				1.08011	0	0.00035275	0.20656
2.8				1.09874	0	0.00021811	0.18194
3				1.1308	0	0.00013387	0.18364
3.25	1.30472	0.00223	0.14476	2.28615	0.15347	9.1971E-05	0.27272
3.5	1.35817	0.00171	0.18984	2.06853	0.13802	5.4529E-05	0.23844
3.75	1.25008	0.00119	0.18048	1.93469	0.13967	3.3548E-05	0.19746
4	0.93909	0.00095937	0.13126	1.90814	0.20161	2.0082E-05	0.05501
4.25	0.88072	0.00071251	0.14632	1.78058	0.21934	1.1933E-05	0
4.5	1.56711	0.00043421	0.249				0.4642
4.75	0.74997	0.00044547	0.12226				0
5	0.83127	0.0003603	0.12263				0.12739

5.5	0.92064	0.00023448	0.16332				0.26163
6	1.4472	0.0001662	0.12484				0.87175
6.5	2.85615	7.7349E-05	0.23081				2.06221
7	2.67006	5.5229E-05	0.21783				1.94861
8	2.39912	3.2101E-05	0.1701				1.82454
9	2.18916	0.00001835	0.16842				1.7086

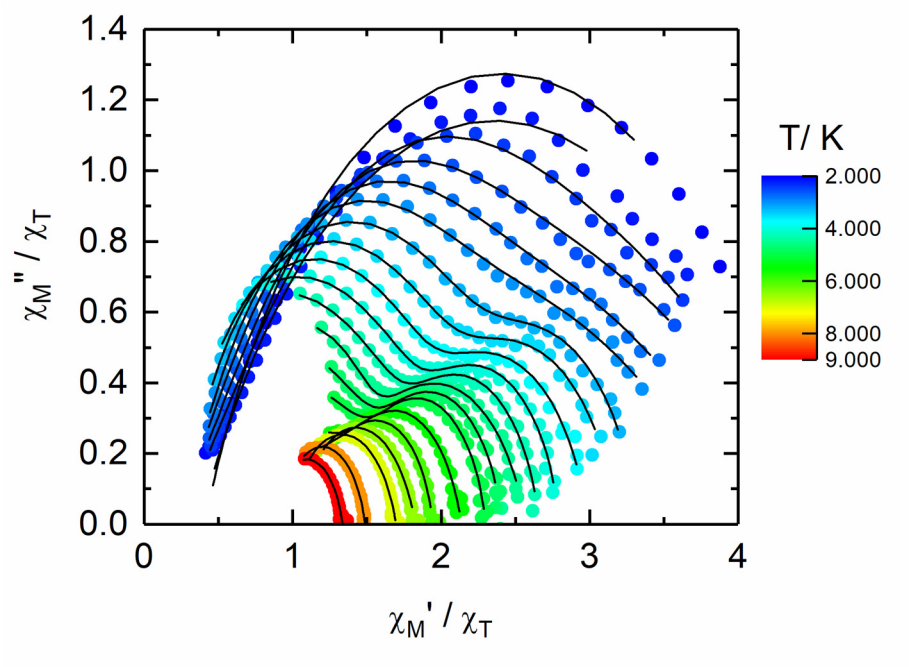

Figure S14. Normalized Argand plot for **2** between 2 and 9 K.

Characterization of 4,7-di-tert-butyl-2-(3,5-di-tert-butyl-4-oxocyclohexa-2,5-dien-1-ylidene)benzo[d][1,3]dithiole-5,6-dione (**L**[1])

^{1}H NMR ($CDCl_3$, 400 MHz): δ 1.34 (s, 18H), 1.49 (s, 18H), 7.15 (s, 2H); ^{13}C{1H} NMR ($CDCl_3$, 100 MHz): δ 29.4, 30.2, 35.6, 37.9, 123.0, 126.0, 141.1, 144.4, 147.8, 148.8, 183.3, 185.7; IR (nujol, cm^{-1}) 1648, 1629, 1605, 1377, 1364, 1331, 1294, 1253, 1221, 1100, 1085, 1029, 978, 891, 881, 838, 818, 766, 722, 674, 534.